THE DISTRIBUTION OF THE 6_2-6_1 AND 5_2-5_1 E-TYPE METHANOL MASERS IN OMC-1

K. J. JOHNSTON, R. GAUME, AND S. STOLOVY

Center for Advanced Space Sensing, Code 4200 Naval Research Laboratory, Washington, DC 20375-5000

T. L. WILSON AND C. M. WALMSLEY

Max-Planck-Institut für Radioastronomie, Auf Dem Hugel 69, 53 Bonn 1, Germany

AND

K. M. MENTEN

Harvard-Smithsonian Center for Astrophysics, 60 Garden Street, MS42, Cambridge, MA 02138

ABSTRACT

The 6_2-6_1 and 5_2-5_1 E transitions of CH_3OH have been mapped toward the Orion-KL region with an angular resolution of 3″ and a frequency resolution of 12 kHz ($=0.15$ km s^{-1}). There are at least 16 masers of flux density greater than 3 Jy. These are distributed in a 40″ long crescent shaped region, extending from NW to SE around the "hot core." The radial velocities and positions of some of these masers agree with a peak of the 8_0-7_1 A transition of CH_3OH, near 95 GHz. The most intense 6_2-6_1 E maser is unresolved; the flux density of 103 Jy and size of less than 1″1 give a brightness temperature of greater than 10^5 K. The FWHP line widths, including the instrumental resolution, range from less than 0.15 km s^{-1} (unresolved) to 1 km s^{-1}. What have been previously cataloged as spatially extended individual masers are most likely blends of maser components with slightly different radial velocities. The E-type masers in Orion appear to cluster on scale sizes of less than 3″. From a multiline analysis and our limits to maser source sizes, the column densities in the regions with the most intense lines are greater than 2×10^{22} cm^{-2}. The spatial distribution and the observed velocities suggest that the methanol masers arise from high column density gas adjacent to the Hot Core. The masers may be located very near the interface of the high-velocity outflow and the surrounding dense gas.

Subject headings: ISM: kinematics and dynamics — ISM: molecules — ISM: structure — masers

1. INTRODUCTION

The Orion Molecular Cloud, OMC-1, is one of the best studied star-forming regions in the Galaxy. The cloud is complex and inhomogeneous. The major features of OMC-1 deduced from maps in various molecular lines indicate regions of different temperatures and densities. The regions in OMC-1 which are relevant to the present study are all near the Orion KL infrared nebula. We enumerate these as follows:

1. The Hot Core, a region rich in complex molecular emission (see, e.g., Jewell et al. 1989), of total size 10″, which is centered 3″ south of the 20 μ source IRc2 (Downes et al. 1981). The Hot Core has an average density, $n(H_2) \sim 10^7$ cm^{-3} and an average kinetic temperature $T_k = 160$ K (see, e.g., Hermsen et al. 1988). The radial velocity is 5.5 km s^{-1}.

2. The high-velocity bipolar CO outflow (Erickson et al. 1982; Olofsson et al. 1982; Wilson, Serabyn, & Henkel, 1986b); outflowing material is also found in water vapor masers (Genzel et al. 1981) and vibrationally excited molecular hydrogen (Beckwith et al. 1978).

3. The compact ridge (radial velocity 8 km s^{-1}), centered 9″ south of IRc2, shows intense quasi-thermal methanol emission. This is referred to as the MEC, or methanol emission core (Menten et al. 1988a, b; Wilson et al. 1989).

Differences in the spatial distribution of various molecular species near Orion KL are believed to be primarily due to excitation conditions but chemical effects could also play a major role in determining the observed spatial distributions.

Some transitions of the E species of CH_3OH near 25 GHz display maser emission, first detected by Barrett, Schwartz & Waters (1971). The spectra of the $J = 6$ and 7 lines were found to consist of narrow features of flux density of order 100 Jy (Hills, Pankonin, & Landecker 1975). The 6_2-6_1 E transition was mapped with a resolution of 6″ by 15″ by Matsakis et al. (1980). The methanol masers were shown to be distributed differently from H_2O or OH masers, and several of these masers were reported to be resolved. The installation of new K-band receivers on the VLA made possible observation of the 25 GHz transition with improved angular resolution and sensitivity; these results are reported here. Since maps of quasi-thermal and maser emission from methanol are available, these data can be combined to limit the range of excitation conditions in the maser line emission regions. It might be possible to relate the parameters of the methanol maser centers to conditions determined from maps of other species.

2. OBSERVATIONS AND RESULTS

All the available antennas of the VLA of the National Radio Astronomy Observatory[1] were used in the D configuration on 1988 August 20. Spectral line observations were made using 64 channels covering the inner half of the observing band which had a width of 1.5625 MHz. The channel separation was 12.2 kHz (0.15 km s^{-1} at the line rest frequency). The methanol lines observed were the 6_2-6_1 E (rest frequency 25018.12 MHz; Lovas 1986) and the 5_2-5_1 E (rest frequency 24959.08 MHz) transitions. The spectral band was centered at 8.0 km s^{-1}, LSR. Right circular polarization was observed. The flux

---

[1] The VLA is a facility of the National Radio Astronomy Observatory operated by Associated Universities Inc., under a cooperative agreement with the National Science Foundation.

232

density scale was established by adopting a flux density for 3C 84 of 42 Jy at the line frequencies.

The measurements were obtained by observing the 6_2–6_1 E line for 12 minutes and the calibrator 0528 + 134 for 8 minutes. The 5_2–5_1 E line was also observed with the calibrator for the same length of time. Observations of these two lines were alternated in this way for an 8 hr period. The calibrator was used to determine the instrumental gains and phases. Using a pixel size of 1″, 256 × 256 pixel maps were made of the 6_2–6_1 E transition. The synthesized beamwith was 3″31 by 2″71, at a position angle of − 18°.

The spectral channel centered at 8 km s^{-1} is dominated by a single intense feature, which has a simple structure. This was used as a model for self-calibration. This channel was also used to determine the positions of maser features in the other spectral channels by referencing their positions to the non–self-calibrated position of the masers in the 8 km s^{-1} channel. After self-calibration, the data were again mapped and CLEANed using the standard procedure in the AIPS package. There was no detectable continuum emission in the channels off the line so that no attempt was made to subtract the continuum emission from the maps. The 5_2–5_1 E transition was treated the same way, except that the cellsize used was 0″8. Spectra of both transitions were obtained by summing the flux density over a 50″ by 50″ square centered on R.A. = 05^{h}32^{m}46^{s}9, Decl. = −05°24′15″0 (1950.0). These are displayed in Figure 1. From the general similarity of these average spectra, we might expect a one-to-one agreement between the individual 5_2–5_1 and 6_2–6_1 maser features in the VLA maps.

The positions of the maser features were determined by fitting two-dimensional Gaussians to the data in the channel maps. The intensity limit for velocity features was adopted to be 3 Jy beam^{-1}. Above this flux density level, individual maser features could be reliably identified. There appears to be a confusing background level of emission at the 3 Jy beam^{-1} level. The theoretical rms sensitivity of these maps (from system temperature, integration time, etc.) is of order 30 mJy. In a 3″ beam, 3 Jy corresponds to a main beam brightness temperature of 730 K. The difference between the theoretical
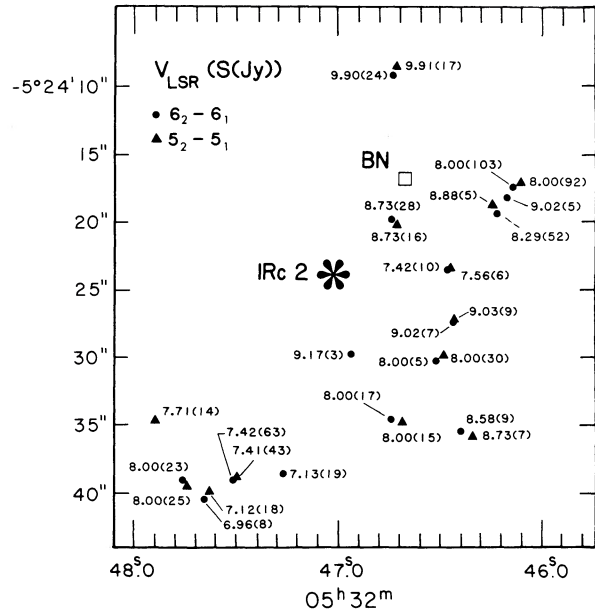
FIG. 2.—Distribution of the CH$_3$OH masers in Orion obtained from two-dimensional Gaussian fits to channel maps. The filled circles denote the 6_2–6_1 E transition while the triangles denote the 5_2–5_1 E transition. The number after the symbol is the radial velocity (with respect to LSR) of the maser feature; the total flux density (in Jy) is given in parentheses. The open box shows the position of the BN source, and the star marks the position of IRc2 (see Downes et al. 1981).

sensitivity and actual limits from Gaussian fitting may indicate the presence of many weak masers. Another possibility would be superthermal (i.e., $T_{ex} > T_k$), optically thick line emission.

In Figure 2, we present a map of the features obtained from fits to the 6_2–6_1 E and 5_2–5_1 E line data. (The flux densities of the individual features are given in parentheses in Fig. 2.) From an inspection of Figure 2, the spatial distribution, total flux density, and radial velocity of the 6_2–6_1 E emission is similar to that of the 5_2–5_1 E transition. The velocity components for both transitions are listed in Tables 1 and 2, ordered by radial velocity. For 11 of 14 features with flux densities greater than 3 Jy, there is a coincidence of 6_2–6_1 with 5_2–5_1 maser spots to within ≈ 1″. The agreement in radial velocity is better than 0.5 km s^{-1} for most features. The most prominent exception is the intense, 52 Jy, feature at 8.3 km s^{-1} in the 6_2–6_1 E transition. The nearest 5_2–5_1 E feature has a radial velocity 0.5 km s^{-1} higher, and a total flux density 10 times lower. The difference in radial velocity may be an indication of the uncertainties in our fitting procedure; the differences in flux density cannot be so explained. Two other examples where one or another transition is missing are the 14 Jy (5_2–5_1 E) maser at 7.71 km s^{-1} and the 5 Jy (6_2–6_1 E) maser at 9.2 km s^{-1}.

The velocity width (FWHP) of these features ranges from 1.0 to less than 0.15 km s^{-1} with the majority less than 0.44 km s^{-1}. The measured sizes range from unresolved to 4″1 by 3″0 for the 7.71 km s^{-1}, 5_2–5_1 E feature. The features with velocity widths greater than one channel, 0.15 km s^{-1}, were mapped in all channels and Gaussian fits made to the features. It was found that for individual channel maps identified with a single maser feature, the positions varied by up to 1″ and that the flux densities were not Gaussian distributed in velocity. This leads us to conclude that those features that appear to be spatially resolved are likely to be a superposition of individual masers and that the typical size of these individual masers is less than
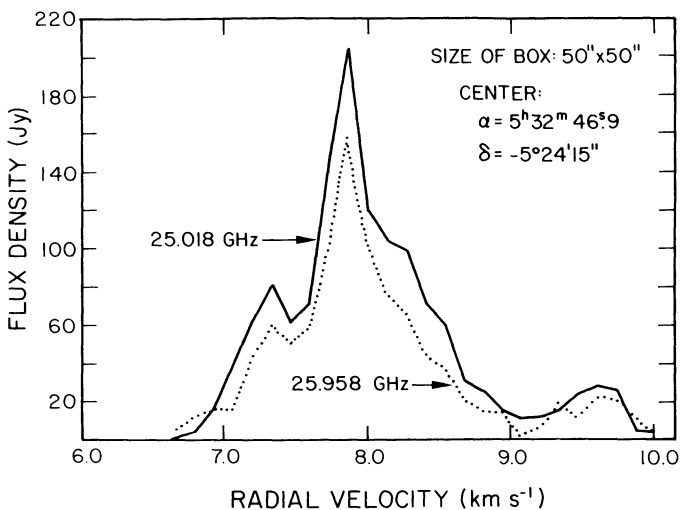
FIG. 1.—Spectra of the 6_2–6_1 E (25.018 GHz) and 5_2–5_1 E (24.959 GHz) transitions of CH$_3$OH in Orion found by summing a 50″ square are centered on R.A. = 05^{h}32^{m}46^{s}9, Decl. = −05°24′15″0 (1950). The radial velocities are with respect to LSR.

TABLE 1

MEASURED PARAMETERS FOR THE 6_2–6_1 E CH$_3$OH MASERS

FEATURE NUMBER	RADIAL VELOCITY (km s^{-1})	WIDTH FWHP (km s^{-1})	POSITION R.A.(1950) (5^h32^m)	POSITION Decl.(1950) ($-05°24'$)	S_{PEAK} (Jy)	S_{TOTAL} (Jy)	FWHP SIZE
1..........	9.90	0.73	46^s.755	09".04	23.4	23.8	<1"
2..........	9.17	0.15	46.945	29.84	2.8	2.6	<1.9
3..........	9.02	0.15	46.182	18.52	4.6	5.4	<2.7
4..........	9.02	0.58	46.429	27.38	5.3	6.8	<3.6
5..........	8.73	0.44	46.744	19.38	28.7	28.2	<1.2
6..........	8.58	0.44	46.399	35.40	6.3	9.4	2.5 by 1.7 p.a. 0°
7..........	8.29	0.73	46.245	19.25	56.9	52	<1.3
8..........	8.00	0.87	46.740	34.66	12.7	17.2	2.5 by 1.2 p.a. 150°
9..........	8.00	0.58	46.511	30.11	5.2	4.9	<1
10........	8.00	0.58	47.769	39.11	22.5	23	<1.5
11........	8.00	0.58	46.147	17.56	100.8	102.9	<1.1
12........	7.42	0.29	46.458	23.39	7.5	10.1	2.2 by 1.6 p.a. 114°
13........	7.42	0.58	47.526	39.00	37.7	62.6	3.4 by 1.0 p.a. 84°
14........	7.13	0.15	47.252	38.40	6.3	19.3	6.2 by 2.7 p.a. 116°
15........	6.96	0.29	47.651	40.57	7.7	8.3	<1.7

1".1, the upper limit to the size of the strongest spectral feature observed here. Spatial blending is evident from an inspection of several of the barely resolved components. For example, the 8.0 and 8.29 km s^{-1}, 6_2–6_1 E features are separated by 2".2; the 7.42 and 6.98 km s^{-1} features are also spatially blended. This would also imply that the masers are clustered, with typical sizes less than our 3" beam.

In order to search for very extended emission not recorded by the VLA and to set limits on the variability of the masers, we compared integrated flux densities with data taken using the 100 m Telescope of the MPIfR in Effelsberg. The 100 m measurements were taken on 1988 September 11–12. The flux density scale was determined by assuming that NGC 7027 has a flux density of 5.8 Jy. The beam size at 25 GHz is 37". The area was mapped using the procedure described by Menten et al. (1988b). The calibration is believed to be accurate to 10%. The spectra obtained were smoothed to a spectral resolution of 12.2 kHz. The 100 m spectra resemble those previously obtained with this telescope by Hills et al. (1975) and Menten et al. (1988b). We therefore conclude, in agreement with Menten et al. (1988b), that there have been no flux density variations of more than 25% in the E-type spectral line profile,

spatially averaged over the entire emission region, between 1975 and 1988. This does not rule out significant variations in the flux densities of individual maser features, which could be spatially and spectrally blended in these lower resolution measurements. A detailed comparison of the 100 m spectra and our VLA spectra was made by smoothing the components listed in Tables 1 and 2 with the 100 m beam. The spectra agree to within 10%. Thus, the VLA has recorded most of the line emission. This comparison also does not rule out the presence of some extended emission or quasi-thermal emission at levels of less than 3 Jy beam^{-1}.

3. DISCUSSION

The highest spatial resolution maps of the CH$_3$OH masers in Orion published to date are those of Matsakis et al. (1980). These were made with a beamsize of 6" in right ascension and 15" in declination. The velocity resolution in their final maps ranged from 0.36 to 0.74 km s^{-1}. The overall morphology of the Matsakis et al. (1980) data is similar to ours. Our maps (Fig. 2) show that the masers are distributed along an arc from northwest to southeast with a velocity variation from 10 km s^{-1} (NW) to 7 km s^{-1} (SE). For the majority of the individual

TABLE 2

MEASURED PARAMETERS FOR THE 5_2–5_1 E CH$_3$OH MASERS

FEATURE NUMBER	RADIAL VELOCITY (km s^{-1})	WIDTH FWHP (km s^{-1})	POSITION R.A.(1950) (5^h32^m)	POSITION Decl.(1950) ($-05°24'$)	S_{PEAK} (Jy)	S_{TOTAL} (Jy)	FWHP SIZE
1..........	9.91	0.72	46^s.744	08".89	16.3	17.4	<1".7
4..........	9.03	0.29	46.412	27.14	5.5	9	<5
3..........	8.88	0.15	46.254	19.11	3.8	5.3	<3.8
5..........	8.73	0.44	46.732	19.19	14.3	15.9	<1.5
6..........	8.73	0.15	46.369	35.81	4.1	6.8	<4.7
11........	8.00	1.03	46.128	17.36	84.5	92	<1.5
9..........	8.00	0.59	46.495	29.95	27	30	<1.7
8..........	8.00	0.44	46.694	34.89	7.5	15.1	3.9 by 2.2 p.a. 133°
10........	8.00	0.59	47.760	39.22	21.4	25	<1.9
16........	7.71	0.15	47.880	34.70	5.9	14.3	4.1 by 3.0 p.a. 81°
12........	7.56	0.29	46.440	23.28	5.1	6.4	<2.5
13........	7.41	0.44	47.527	38.98	22.4	43.1	3.9 by 1.6 p.a. 95°
15........	7.12	0.29	47.624	40.03	8.3	18	<6.1

features, the maps agree in position to within the combined errors for the intense features; larger disagreements occur for weaker features. The intensities of a few of the strongest features appear to disagree. Our strongest feature at 8.0 km s^{-1} is located at R.A. = $05^h32^m46^s.147$, Decl. = $-05°24'17".56$ (1950.0). Matsakis et al. (1980) report that the most intense feature is 7.3 km s^{-1} and is located at R.A. = $05^h32^m47^s.6$, Decl. = $-5°24'39"$ (1950.0). This corresponds to our 7.42 km s^{-1} feature in Table 1 which is the second most intense component. Since, as already stated, our results show good agreement with the single dish measurements of Hills et al. (1975), Menten et al. (1988b) and unpublished data obtained in 1988 September, we cannot attribute the apparent change in intensity in these as being caused by large time variations. Future high spatial resolution measurements are needed to ascertain the extent of the variability of individual masers.

Matsakis et al. (1980) concluded that the more intense

masers were spatially resolved, with sizes of $6"-8"$. However, this conclusion is not supported by our maps. In light of our higher resolution data, we conclude that the maps of Matsakis et al. (1980) as well as those presented here are affected by confusion. The strongest feature reported by Matsakis et al. (1980) is the 7.42 km s^{-1} feature, for which we measure a size of $\sim 3" \times 1"$. We assume that this is a blend of several features. As discussed above, our higher angular resolution gives brightness temperatures which are also considerably higher than those found by Matakis et al. (1980). For example, the brightness temperature of the strongest (8.0 km s^{-1}) feature is greater than 2×10^5 K ($< 1".1$ size and 103 Jy flux density). For some velocity features listed in Table 1, we give sizes rather than limits. These are probably due to spatial and spectral blending of unresolved features; there are no individual masers truly larger than the synthesized beam. Thus, all of the brightness temperatures found from this study are *lower limits* because none of the features are resolved.

A comparison with other transitions of methanol, in Figure 3, shows that the CH$_3$OH masers arise from the same general region as the quasi-thermal transitions from the 10_1-9_2 A^-
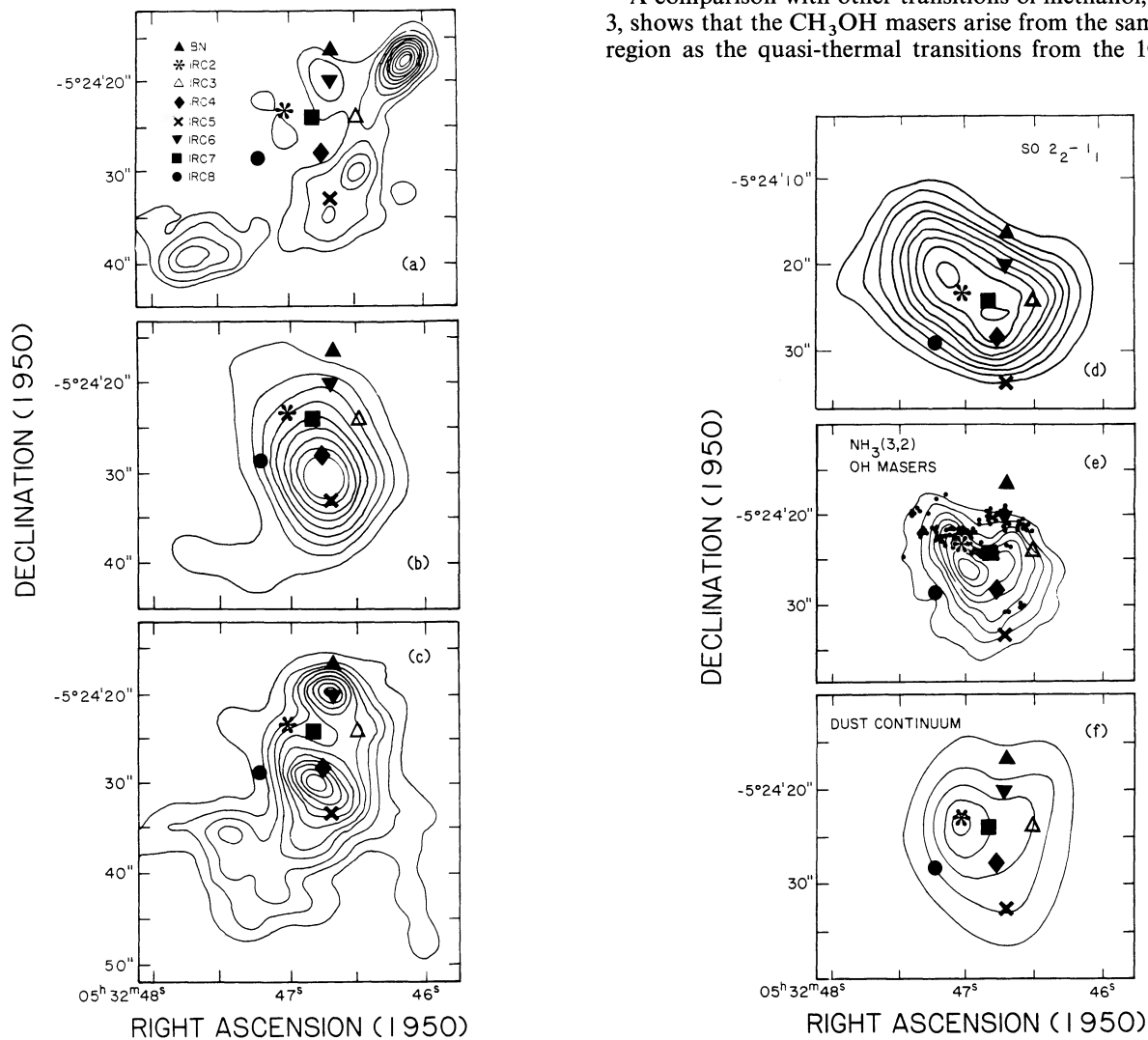
FIG. 3.—Comparison of high angular resolution maps of various species in the Orion-KL region with the CH$_3$OH maser data. (*a*) the IR continuum sources are identified in the left side of this panel. The contours show the velocity integrated emission from the 6_2-6_1 E transition. (*b*) The contours of the quasi-thermally excited 10_1-9_2 A^- transition of methanol, from Wilson et al. (1989). (*c*) The contours of emission from the 8_0-7_1 A^+ transition of methanol, from Plambeck & Wright (1988). (*d*) The contours of emission from the SO 2_2-1_1 line, from Plambeck et al. (1982). (*e*) The contours of thermally excited emission from NH$_3$(3, 2) emission (Migenes et al. 1989); the filled circles mark the location of the OH 1665 MHz maser emission (Johnston et al. 1989). (*f*) The contours of dust emission, measured at 3 mm (Masson et al. 1985).

levels (6″ resolution; see Fig. 3b Wilson et al. 1989), and the 5_1–4_0 E levels (Menten et al. 1988a). We do not show the 5_1–4_0 E map, because this transition was mapped with a 26″ resolution. The intensity distribution in the latter map has a Gaussian shape; this must be due to the large beam width used in that study. None of the methanol masers are located at the highest intensity peak of quasi-thermal methanol emission, 9″ south of IRc2. All of the E-type CH_3OH maser emission is contained within the region from which the low-excitation quasithermal 5_1–4_0 E emission arises, but the northwest maximum of the E-type methanol maser emission is beyond the lowest contour of the map of the high-excitation 10_1–9_2 A^- transition (Wilson et al. 1989). This may indicate a gradient in the excitation of the E-type methanol maser centers, if there is no structure in the 10_1–9_2 A^- emission on scales much smaller than 10″.

The only map of another methanol transition with a comparable angular resolution is that of the 8_0–7_1 A^+ transition at 95 GHz (4″ resolution; Fig. 3c; Plambeck & Wright 1988). The spatial distributions of the 8_0–7_1 A^+ and 6_2–6_1 E transitions are somewhat similar. As noted by Plambeck & Wright (1988), the northern feature at 8.4 km s^{-1} (also coincident with IRc6) arises from a very small region and is believed to be due to maser emission. The strongest feature of the 6_2–6_1 E transition does not coincide with this maser, but there is a much weaker 6_2–6_1 E-type maser feature (of order 20 Jy) at 8.7 km s^{-1} at this position. It is very difficult to make a detailed association of our CH_3OH emission (Fig. 3a) with the "plume" (Fig. 3b and Fig. 3c), located southwest of IRc4. Features 10, 13, 15, and 16 in Table 1 are nearby but not quite coincident with this feature. Plambeck & Wright (1988) had favored a quasi-thermal origin for this emission. From the general similarity of our map of maser line emission to that of the 8_0–7_1 A^+ emission, one might conclude that *all* of the emission in these two transitions is due to maser emission. But there is also good agreement with the 10_1–9_2 A^- map (Fig. 3b), which is thought to be caused by a quasi-thermal line emission process. One must conclude that part of the 8_0–7_1 A^+ line emission is caused by masering, and part by quasi-thermal emission.

Comparisons with maps of other species show a marked disagreement of the distribution of the 25 GHz E-type masers with the 2_2–1_1 transition of SO (Fig. 3d Plambeck et al. 1982), the (3, 2) transition of NH_3 (Fig. 3e, Migenes et al. 1989) and the dust continuum (Fig. 3f, Masson et al. 1985). The latter two maps delineate the hot core region, whereas the CH_3OH masers *avoid* the hot core. This may be caused by turbulent gas motions which limit the maser intensities.

Matsakis et al. (1980) noted that there was a rough correspondence between the methanol masers positions and the peaks of 2μ vibrationally excited H_2 emission, hereafter H_2^*. In Figure 4 we have superposed the velocity averaged map of the 5_2–5_1 E emission (*Shaded area*) on contours of 2μ H_2 emission (Fischer et al. 1991) and a dotted line which represents the boundary of the Hot Core (see, e.g., Migenes et al. 1989). The different maps in this overlay are consistent with the earlier results of Matsakis et al. (1980) and Beckwith et al. (1978). The higher quality of these newer data make the following interpretation more secure. The orientation of the methanol maser emission is similar to that seen at the southern edge of the map of 2μ H_2^* but there is, for example, no obvious maser counterpart of the two peaks in H_2^* north and the peak east of the CH_3OH distribution. The 2μ H_2^* line is emitted from regions of strongly shocked gas. This is probably due to the interaction of

the bipolar outflow with high-density clumps. It is possible that the methanol maser emission is also an interface indicator. A necessary condition of the methanol maser emission is coherence along the line of sight. Given the high degree of turbulence in the Orion region, this condition cannot be fulfilled everywhere. It is possible, for example, that methanol maser emission only occurs in shocked regions if the shock velocity is nearly perpendicular to the line of sight. It is important to note that the observed methanol velocities are close to those observed towards "quiescent" gas in this neighborhood (see, e.g., the $C^{18}O$ data of Wilson et al. 1986a). This is difficult to understand if the methanol emission is supposed to originate in shock-excited gas. However, this would be compresensible if the shocks in question were perpendicular to the line of sight. In Figure 5 we show a sketch of the Orion outflow region. The methanol masers are assumed to be located behind the shocked gas. The shocks are caused by the interaction of the high speed outflow (seen in CO) with quiescent gas. In order to produce detectable maser lines, the gas motions must be at right angles to the line of sight. In this picture, the H_2^* shows the shocked gas interface. The methanol masers are present in smaller regions where the fortuitous line-of-sight geometry allows the maser lines to grow in intensity.

We next discuss the excitation of the individual 5_2–5_1 E and 6_2–6_1 E masers as a prelude to estimating abundances in the maser regions. The methanol masers have components which have angular sizes less than 1.1 (linear sizes less than 1×10^{16} cm at 500 pc). Correspondingly, the maser brightness temperatures are greater than 1×10^5 K. This suggests that, unless the masers are highly beamed, the masers are saturated. A rough condition for saturation is

$$\frac{\Omega k T_b}{4\pi h\nu} A > \Gamma , \tag{1}$$

where T_b is the peak brightness temperature of the 6_2–6_1 maser
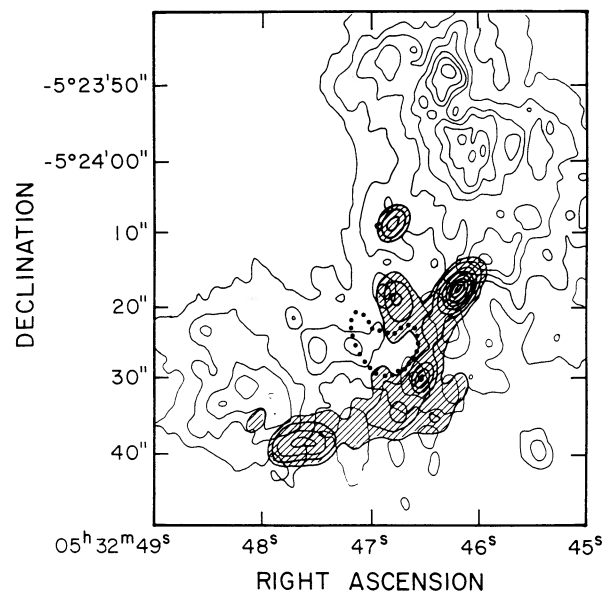
FIG. 4.—Contours show the distribution of molecular hydrogen emission at 2μ from the $v = 1$–0 S(1) emission line (Fischer et al. 1991). The shaded contours represent the emission from the 5_2–5_1 E transition of CH_3OH, integrated over velocity. The lowest contour of the NH_3 emission from the Hot Core is shown as a dotted line.

H$_2$O MASERS

Hi-V CO   OH MASERS

SO

CO

HOT CORE

THERMAL
CH$_3$OH
AND H$_2$CO
PEAK   H$_2$O

CH$_3$OH   SHOCKED
MASERS   H$_2$, H$_2^*$
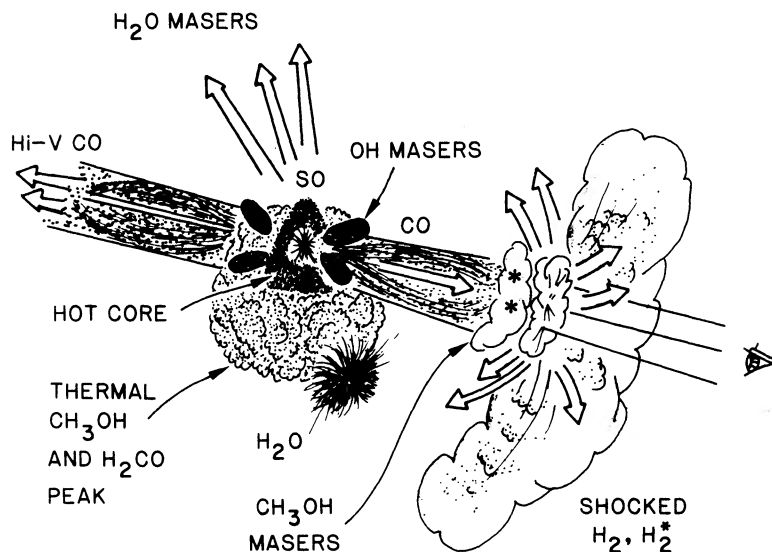
Fig. 5.—Possible representation of clouds in the OMC-1 region. The dimensions are not to scale. The outflow denoted by the CO emission appears to emanate near IRc2. The emission plows into a quiescent cloud causing the molecular hydrogen emission. The methanol maser emission arises from a cloud just behind the molecular hydrogen emission.

line, A is the spontaneous transition rate of the maser line $(8.3 \times 10^{-8}$ s$^{-1})$, $h\nu/k$ is the transition energy, 1.20 K, and Γ is the level decay rate (of order 3×10^{-4} s^{-1}). We have no estimate of the magnitude of maser beaming, but if we take $\Omega/4\pi$ to be ~ 0.1, we find we find that saturation is probable for brightness temperatures above 4×10^4 K. Our observed brightness temperatures are higher than this in several components. Saturation is also consistent with the observed slow or nonvariability of the Orion masers over the past few years. All these arguments favor, but definitely do not prove, that the Orion methanol masers are saturated; a quantitative investigation of this question involves higher angular resolution observations.

For the strong maser lines, this result also implies optical depths of at least 10 (in absolute value). With this value, we can derive very rough physical parameters for the methanol maser spots. To do this, we first note that the column density in the lower level of the 6_2–6_1 transition is given by

$$N_6/T_{ex} = 1.586 \times 10^{13}\tau\,\Delta V\,, \qquad (2)$$

where ΔV is the FWHP line width in km s^{-1} and τ is the line optical depth. T_{ex} is the line excitation temperature of the maser transition which is a function of the relative populations of the energy levels involved. The quantity T_{ex} is unknown but a reasonable estimate is between -1 and -10 K corresponding to an overpopulation of upper relative to lower level between 10% and 100%. For T_{ex} between -10 and -1 and $\Delta V = 0.5$ km s^{-1}, we have N_6 between 1×10^{14} and 1×10^{15} cm^{-2}. By examining the dependence of the Orion methanol masers upon excitation, Menten et al. (1988b) concluded that the relative populations of the maser lower levels could be described by a temperature of 80–100 K. Then, roughly 0.6% of the population is in the 6_1 level. The total methanol column density must be in the range 2×10^{16} to 2×10^{17} cm^{-2}. Since the diameter of the maser components is less than 10^{16} cm, we conclude that the methanol number density is at least 2 cm^{-3}. The CH$_3$OH abundance relative to H$_2$ is unknown. To estimate the minimum H$_2$ density, we take the high end of the relative abundance range 1×10^{-6} to 3×10^{-9} found by

Menten et al. (1988a) for thermally excited methanol. Then the H$_2$ number density must be at least 2×10^6 cm^{-3} in the maser region and the H$_2$ column density at least 2×10^{22} cm^{-2}. Although these estimates have (perhaps) order of magnitude uncertainties, these lower limits are likely to be conservative.

While we have obtained a lower limit to the H$_2$ density in the maser region, other considerations suggest that the H$_2$ density is unlikely to be much above 1×10^8 cm^{-3} and that the 25 GHz masers are probably collisionally pumped. This statement is based on the "family resemblance" of the J_2–J_1 masers to the so-called "class A" masers found at 36 GHz $(4_{-1}$–3_0 $E)$, 84.5 GHz $(5_{-1}$–4_0 $E)$, 44 GHz $(7_0$–6_1 $A)$, and 95 GHz $(8_0$–7_1 $A)$. This family of transitions appear in general (although not always) to show maser emission from the same positions. Moreover, statistical equilibrium calculations show that such simultaneous maser action can be understood for a range of excitation conditions assuming purely collisional excitation (see Morimoto, Ohishi, & Kanzawa (1985), and Walmsley et al. (1988) for details of the statistical equilibrium models). The properties of the "class A" masers have been recently discussed by Haschick, Menten, & Baan (1990) who carried out a survey in the 44 GHz line. 25 GHz masers have been found to be coincident with the other "class A" methanol masers in the DR 21(W) and NGC 6334 $-$ I(N) sources (see Plambeck & Menten 1990; Menten & Batrla 1989) but not, for example, in DR 21(OH) which is another standard "class A" source. The reasons for this are not clear, but the data do suggest that in several sources, the J_2–J_1 and the other "class A" maser lines form in the same regions and hence that there is an overlap in the physical conditions required for all of these different "class A" maser lines. In Orion, as we have noted above, at least one 6_2–6_1 maser component coincides with the 95 GHz 8_0–7_1 A^+ maser spot found by Plambeck & Wright (1988). Hence, since the other "class A" masers can be explained with a collisional model, it seems likely that the 25 GHz lines are collisionally pumped. Moreover, since the other lines are quenched at densities of 10^8 cm^{-3} and above, it seems plausible that the density in the J_2–J_1 maser regions is also of the order of or below this limit.

These latter statements can be verified by detailed statistical equilibrium calculations. The main difficulty is the uncertainty of collisional rates. In particular, consideration of the J_2–J_1 series of 25 GHz methanol lines requires an estimate of the relative probabilities for collisional transitions causing changes of 2 and 3 in the k quantum number. As an illustration of what could be true, we have carried out the computations whose results are shown Figure 6. The basic assumptions underlying the model used have been outlined by Walmsley et al. (1988) and by Menten et al. (1988a). The collisional rates used are based upon the experimental results of Lees & Haque (1974) but we have made the arbitrary additional assumption that $|\Delta k| = 3$ collisional transitions occur with a rate which is 10% of that deduced from the Lees & Haque (1974) results for $\Delta k = 0$. $\Delta k = 2$ collisional changes, in contrast, are assumed to be forbidden. This assumption causes collisional transition from the $k = 1$ backbone ladder of E-type methanol to $k = 2$ to be relatively likely and hence causes and overpopulation of $k = 2$ relative to $k = 1$. That such a preference for $|\Delta k| = 3$ transitions occurs is plausible given the threefold symmetry of methanol. However, this selection rule is ad hoc. In Figure 6, we plot the optical depth (for a spherically symmetric model in the large velocity gradient approximation) against molecular hydrogen density for an assumed kinetic temperature of 80 K and an assumed methanol abundance of 10^{-7} cm^{-3}. As mentioned above, the masers are quenched at densities above 3×10^7 cm^{-3}. As this model is applied in the case of Orion, it is interesting that the 4_{-1}–3_0 E masers (at 36 GHz) and 5_{-1}–4_0 E masers (at 84 GHz) are quenched at lower densities than the J_2–J_1 lines. These lines appear to be quasithermally excited in Orion, suggesting that the density needed is $\approx 2 \times 10^7$ cm^{-3}. This result is consistent with the estimate obtained from the geometric argument in the previous paragraph. This gives some confidence in our calculation, but in view of the uncertain collisional rates, one should be cautious about applying a very detailed interpretation of Figure 6. However, this diagram gives a qualitative explanation of the J_2–J_1 maser excitation.

From the discussions above, it seems reasonable that in the methanol maser regions, the H_2 density is 10^7 cm^{-3}. Then we find that the fractional methanol abundance is $\sim 10^{-6}$ to $\sim 10^{-7}$. This is a very large relative abundance of methanol, compared to estimates made for dark clouds. One method to produce such an abundance might involve liberating methanol from grain surfaces (see Brown, Charnley, & Millar 1988). This is consistent with the partial agreement of vibrationally excited H_2 and methanol masers, in Figure 4. Then we expect the methanol to be present in postshock regions. The methanol masers we have mapped could arise in those regions behind the line of sight. In general, the three necessary conditions for the maser emission are (1) a large abundance of the molecule, (2) the appropriate local conditions for inversion of the population, and (3) velocity coherence along the line of sight. For the specific case of methanol, from our results, we can conclude that the H_2 density is an appropriate value $\sim 10^7$ cm^{-3}, local methanol abundance is ~ 1–2 cm^{-3}, and the line of sight velocity dispersion is less than a few km s^{-1}.
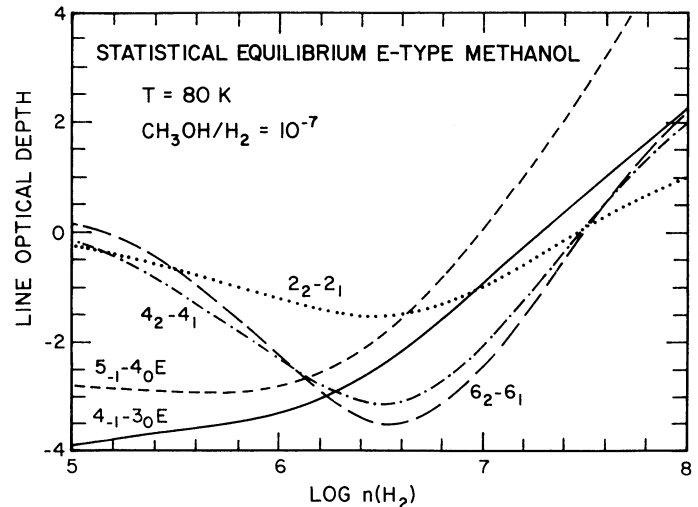
FIG. 6.—Plot of the peak optical depths of various methanol transitions as a function of H_2 density using the large velocity gradient approximation. The kinetic temperature is fixed at 80 K. The $|\Delta k| = 3$ collisional rate is assumed to be 10% of the $\Delta k = 0$ rate (see text).

4. CONCLUSIONS

The 6_2–6_1 E and 5_2–5_1 E transitions of CH$_3$OH in Orion have been mapped and shown to lie over an area of approximately 40″ as previously shown by Matsakis et al. 1980; a detailed comparison shows a qualitative agreement of the intensities and sizes with the previous map. In 11 of 14 cases, the positions, flux densities and radial velocities of the 6_2–6_1 E and 5_2–5_1 E maser components agree. Although individual maser emission regions are unresolved in our 3″ beam, the variation of position with velocity within what is thought to be a single feature implies clustering of masers on scales of less than 3″. The most intense feature has a brightness temperature in excess of 10^5 K. The best agreement is within the map of the 8_0–7_1 A transition of methanol. The masers are located within the lowest contour, but not toward the maxima, of lower excitation quasi-thermal methanol emission. The best spatial correlation is with the distribution of the vibrationally excited H_2 emission. There is a significant anticorrelation with the location of the Hot Core. We hypothesize that the methanol masers are formed behind shock fronts, and that these shocks are moving at right angles to the lines of sight. Presumably, the locations of the masers is determined by three requirements, namely, a high abundance of methanol, low turbulence to allow the maser line intensities to grow, and H_2 densities of order 10^7 cm^{-3}, to provide a maser pump source.

REFERENCES

Barrett, A. H., Schwartz, P. R., & Waters, J. W. 1971, ApJ, 168, L101
Batrla, W., & Menten, K. M. 1988, ApJ, 329, L117
Beckwith, S., Persson, S. E., Neugebauer, G., & Becklin, E. E. 1978, ApJ, 223, 464
Brown, P. D., Charnley, S. B., & Millar, T. J. 1988, MNRAS, 231, 409

Downes, D., Genzel, R., Becklin, E. E., & Wynn-Williams, C. G. 1981, ApJ, 244, 869
Erickson, N. R., Goldsmith, P. F., Snell, R. L., Berson, R. L., & Huguenin, G. R. 1982, ApJ, 261, L103
Fischer, J., Smith, H., & Whitis, M., 1991, in preparation

Genzel, R., Reid, M. J., Moran, J. M., & Downes, D. 1981, ApJ, 244, 844
Haschick, A. D., Menten, K. M., & Baan, W. A. 1990, ApJ, in press
Hermsen, W., Wilson, T. L., Walmsley, C. M., & Henkel, C, 1988, A&A, 201, 285
Hills, R., Pankonin, V., & Landecker, T. L. 1975, A&A, 39, L149
Jewell, P. R., Hollis, J. M., Lovas, F. J., & Snyder, L. E. 1989, ApJS, 70, 83
Johnston, K. J., Migenes, V., & Norris, R. 1989, ApJ, 341, 847
Lees, R. M., & Hague, S. S. 1974, J. Phys., 52, 2250
Lovas, F. J. 1986, J. Phys. Chem. Ref. Data, 15, 251
Masson, C. R., et al. 1985, ApJ, 283, L37
Matsakis, D. N., Cheung, A. C., Wright, M. C. H., Askne, J. I. H., Townes, C. H., & Welch, W. J. 1980, ApJ, 169, 271
Menten, K. M., & Batrla, W. 1989, ApJ, 341, 839
Menten, K. M., Walmsley, C. M., Henkel, C., & Wilson, T. L. 1988a, A&A, 198, 253

Menten, K. M., Walmsley, C. M., Henkel, C., & Wilson, T. L. 1988b, A&A, 198, 267
Migenes, V., Johnston, K. J., Pauls, T. A., & Wilson, T. L. 1989, ApJ, 347, 294
Morimoto, M., Ohishi, M., & Kanzawa, T. 1985, ApJ, 288, L11
Olofsson, H., Elder, J., Hjalmarson, A., & Rydbeck, G. 1982, A&A, 113, L18
Plambeck, R. L., & Menten, K. 1990, ApJ, 364, 555
Plambeck, R. L., Wright, M. C. H., Welch, W. J., Bieging, J. H., Baud, B., Ho. P. T. P., & Vogel, S. N. 1982, ApJ, 259, 617
Plambeck, R. L., & Wright, M. C. H. 1988, ApJ, 330, L61
Walmsley, C. M., Batrla, W., Matthews, H. E., & Menten, K. M. 1988, A&A, 197, 271
Wilson, T. L., Johnston, K. J., Henkel, C., & Menten, K. M. 1989, A&A, 214, 321
Wilson, T. L., Serabyn, E., & Henkel, C. 1986b, A&A, 167, L17
Wilson, T. L., Serabyn, E., Henkel, C., & Walmsley, C. M. 1986a, A&A, 158, L1